TI Designs
*LIDAR*パルス*ToF*リファレンス・デザイン

概要

このリファレンス・デザインは、時間/デジタル・コンバータ(TDC)、および関連するフロントエンドを基礎とする、LIDARの時間測定バックエンドを設計する方法について示します。

リソース

TIDA-00663	デザイン・フォルダ
TDC7200	プロダクト・フォルダ
OPA857	プロダクト・フォルダ
TLV3502	プロダクト・フォルダ
UCC27321	プロダクト・フォルダ
TPL0202	プロダクト・フォルダ
TPS22968	プロダクト・フォルダ
SN74LVC2G14	プロダクト・フォルダ
SN74LVC1G08	プロダクト・フォルダ

E2E™エキスパートに質問

特長

- LIDARのパルス式タイム・オブ・フライト(ToF)測定
- システム・レベルでの距離分解能は1cm未満
- TDC分解能は1.65cmで、ホワイト・ノイズは1.05cm RMS
- TXエネルギー: 40nsにわたってピーク70W

アプリケーション

- ファクトリ・オートメーションの光学近接センサ
- ファクトリ・オートメーションの光学レベル・センサ
- ファクトリ・オートメーションの体積スキャナ
- ドローン
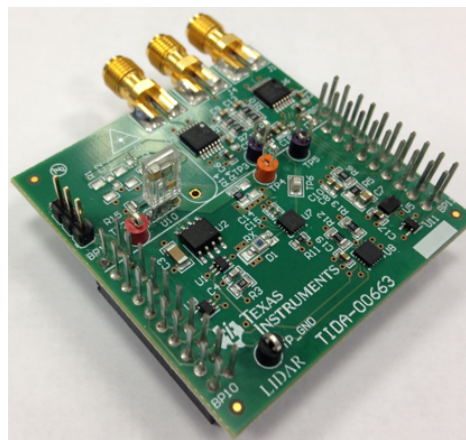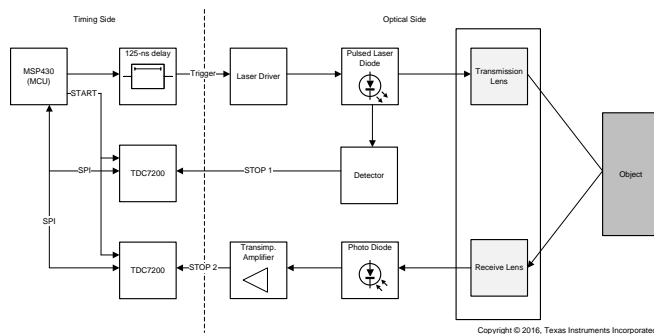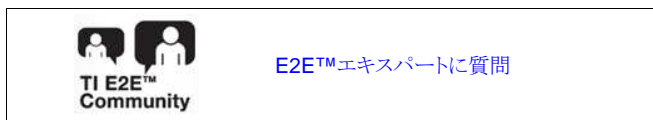
1 System Description

Many applications cannot measure distance to the target by establishing a physical contact. Typical examples include measuring presence of objects on a conveyor belt in logistic centers, ensuring safety distances around moving robot arms, and many others. Possible options for contactless distance measurement are eddy currents, ultrasounds, and light.

Light distance and ranging (LIDAR) systems use the time taken by the light to fly back and forth to an object in an effort to measure the distance to this target. Building a LIDAR system can be made with either a high-speed analog-to-digital converter (ADC) or a time-to-digital converter (TDC).

This reference design shows how to design the time measurement back-end for LIDAR based on a TDC as well as an associated front-end.

1.1 Key System Specifications

表 1. Key System Specifications

PARAMETER	SPECIFICATIONS	DETAILS
ToF measurement	Pulse ToF	2.3.1
ToF resolution	55 ps	Single shot
ToF accuracy		2.3.3
ToF repeatability	35 ps	2.3.3
TX power peak	70 W	
TX pulse width	40 ns	
TX pulse rise time	10 ns	
Max distance	> 100 m[1]	2.3.2
Sampling rate	> 50 kHz	
SNR	88 dB	By design (2.3.4)

[1] End system performance may vary depending on optics selected.

2   System Overview
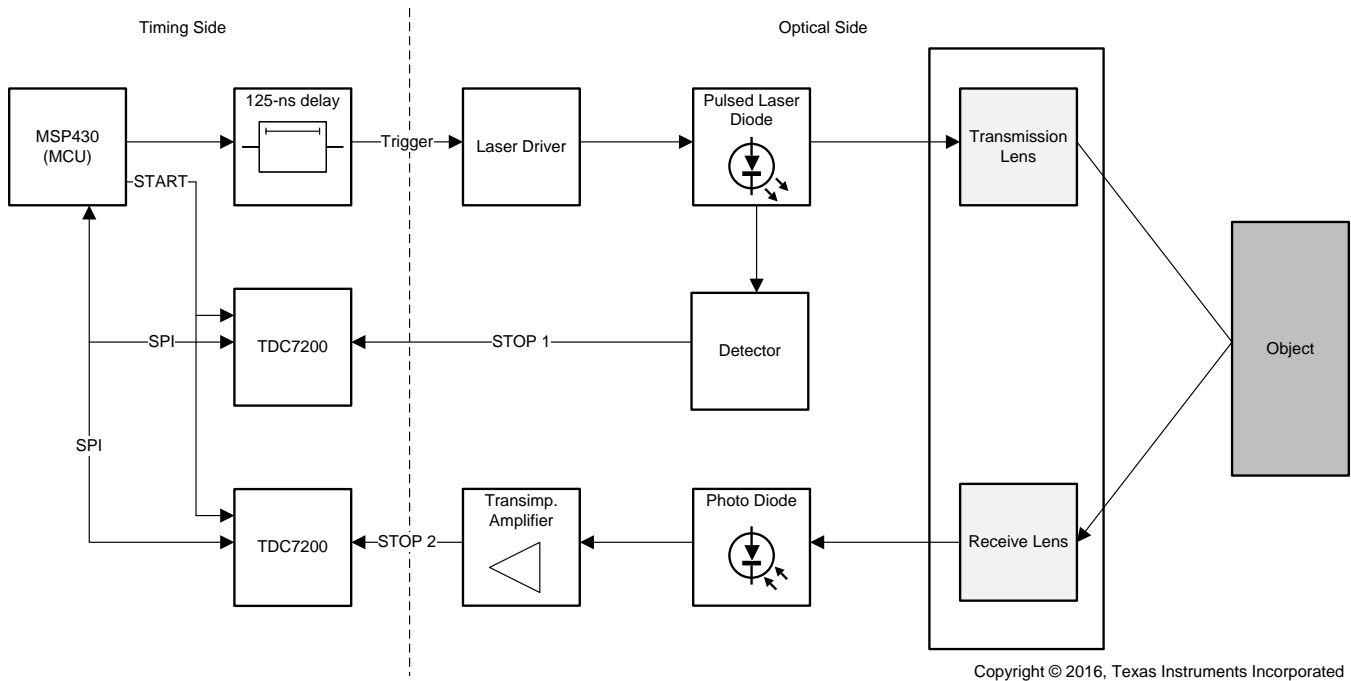
2.1   Block Diagram

図 **1. TIDA-00663 Block Diagram**

2.2   Highlighted Products

2.2.1   **TDC7200**

Features:

- Resolution: 55 ps

- Standard deviation: 35 ps

- Measurement range:
    – Mode 1: 12 ns to 500 ns
    – Mode 2: 250 ns to 8 ms

- Low power consumption: 0.5 µA (2 SPS)

- Supports up to five STOP signals

- Autonomous multi-cycle averaging mode for low power consumption

- Supply voltage: 2 to 3.6 V

- Operating temperature –40°C to +85°C

- SPI host interface for configuration and register access

The TDC7200 is a TDC for ultrasonic sensing measurements such as water flow meters, gas flow meters, and heat flow meters. When paired with the TDC1000 (ultrasonic analog-front-end), the TDC7200 can be a part of a complete TI ultrasonic sensing solution that includes the MSP430™, power, wireless, and source code.

The TDC performs the function of a stopwatch and measures the elapsed time (time of flight or ToF) between a START pulse and up to five STOP pulses. The ability to measure from a START pulse to multiple STOP pulses gives users the flexibility to select which STOP pulse yields the best echo performance.

The device has an internal self-calibrated time base, which compensates for drift over time and temperature. Self-calibration enables time-to-digital conversion accuracy in the order of picoseconds (ps). This accuracy makes the TDC7200 ideal for flow meter applications, where zero and low flow measurements require high accuracy.

When placed in the Autonomous Multi-Cycle Averaging Mode, the TDC7200 can be optimized for low system power consumption, making it ideal for battery powered flow meters. In this mode, the host can go to sleep to save power, and it can wake up when interrupted by the TDC upon completion of the measurement sequence.
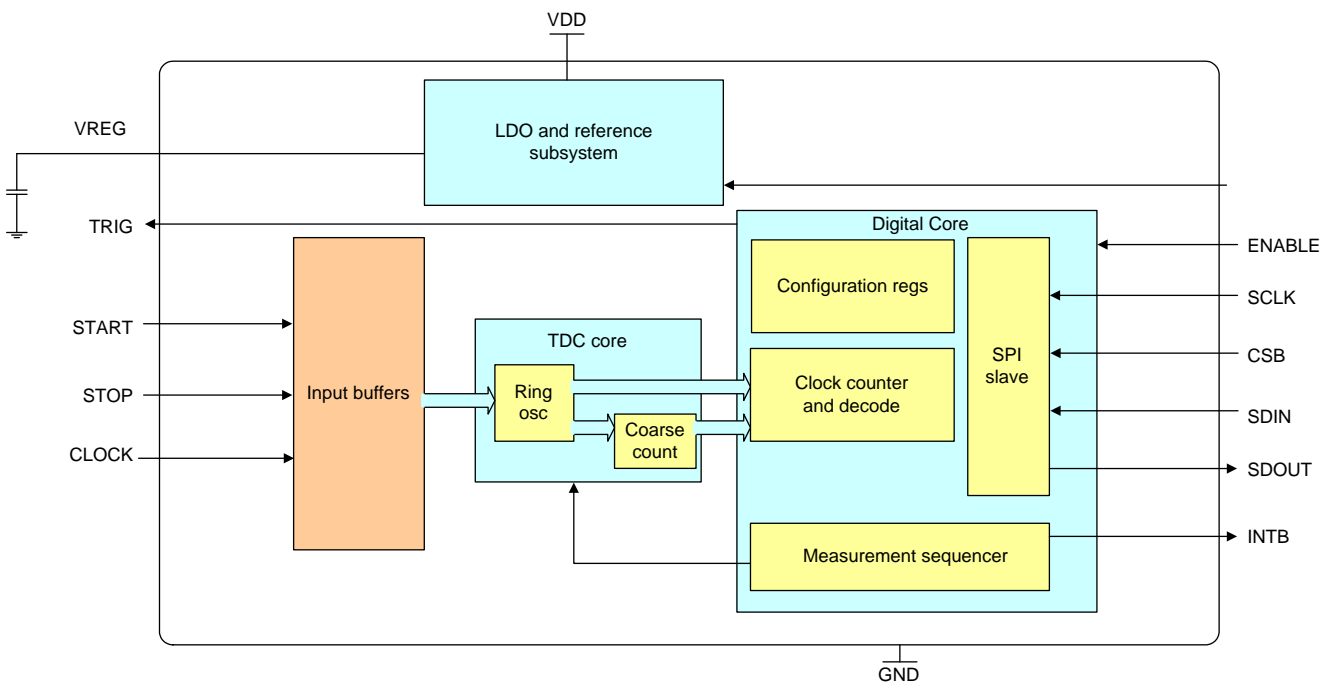
Copyright © 2016, Texas Instruments Incorporated

図 2. TDC7200 Block Diagram

2.2.2   OPA857

Features:

- Internal midscale reference voltage

- Pseudo-differential output voltage

- Wide dynamic range

- Closed-loop transimpedance bandwidth:

    – 125 MHz (5-kΩ transimpedance gain, 1.5-pF external parasitic capacitance)

    – 105 MHz (20-kΩ transimpedance gain, 1.5-pF external parasitic capacitance)

- Ultra-low input-referred current noise (Brickwall filter BW = 135 MHz):
  15 nA$_{RMS}$ (20-kΩ Transimpedance)

- Very fast overload recovery time: < 25 ns

- Internal input protection diode

- Power supply:

    – Voltage: 2.7 to 3.6 V

    – Current: 23.4 mA

- Extended temperature range: –40°C to +85°C

The OPA857 is a wideband, fast overdrive recovery, fast-settling, ultra-low-noise transimpedance amplifier targeted at photodiode monitoring applications. With selectable feedback resistance, the OPA857 simplifies the design of high-performance optical systems. Very fast overload recovery time and internal input protection provide the best combination to protect the remainder of the signal chain from overdrive while minimizing recovery time. The two selectable transimpedance gain configurations allow high dynamic range and flexibility required in modern transimpedance amplifier applications. The OPA857 is available in a 3-mm×3-mm VQFN package.

The device is characterized for operation over the full industrial temperature range from –40°C to +85°C.
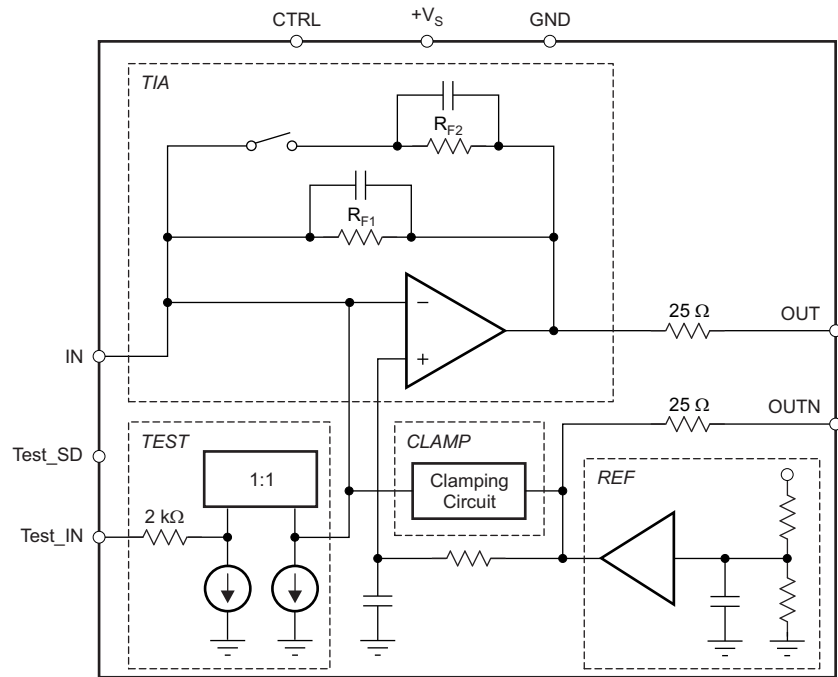
Copyright © 2016, Texas Instruments Incorporated

図 **3. OPA857 Block Diagram**

2.2.3 TLV3502

Features:

- High speed: 4.5 ns

- Rail-to-rail I/O

- Supply voltage: 2.7 to 5.5 V

- Push-pull CMOS output stage

- Shutdown (TLV3501 only)

- Micro packages: 6-pin SOT-23 (single), 8-pin SOT-23 (dual)

- Low supply current: 3.2 mA

The TLV350x family of push-pull output comparators feature a fast 4.5-ns propagation delay and operation from 2.7 to 5.5 V. Beyond-the-rails input common-mode range makes it an ideal choice for low-voltage applications. The rail-to-rail output directly drives either CMOS or TTL logic.

Microsize packages provide options for portable and space-restricted applications. The single (TLV3501) is available in 6-pin SOT-23 and 8-pin SO packages. The dual (TLV3502) comes in the 8-pin SOT-23 and 8-pin SO packages.
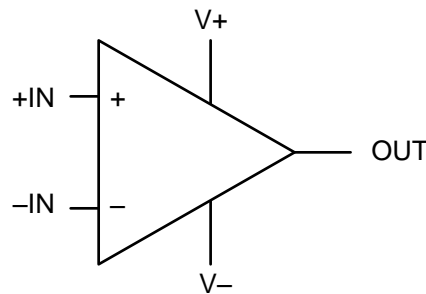
Copyright © 2016, Texas Instruments Incorporated

図 **4. TLV3502 Block Diagram**

2.3 System Design Theory

From a very high level, the system measures the distance between the sensor and the first obstacle ahead of it. The distance is measured by counting the time between the emission of a pulse of light and the reception of the echo. The time measurement is realized by a TDC that can be seen as a stopwatch integrated in a device. The TDC has a timing resolution of 50 ps.

2.3.1 LIDAR System Options

2.3.1.1 Phase Shift Method for ToF Estimation

The phase shift method relies on modulating the amplitude of the light emitted and measuring the phase difference between the emitted light and the received light. Given the speed of light (c) and the modulation frequencies (f), aliasing will happen at distances (d) that are a multiple of d = c × f/2.

To reduce the impact of this effect, multiple frequencies can be used to increase the sensing range. Phase shift measurement can be either direct sampling, heterodyne (because the phase of the signal is not changed at intermediate frequency) or under sampled with I/Q demodulation.

2.3.1.2 Pulse ToF Estimation

The pulse ToF estimation makes a direct measure of the ToF between emission of the laser light and receiving it.

2.3.2 Optical Design

At a high level, the optic design needs to fulfill the following requirements:

- The field of view common between the transmit path and the receive path needs to be as big as possible.
- The optics need to maximize the energy received by the target before it is reflected back to the sensor.
- The optics need to maximize the energy received by the photodiode.
- The optics may have a function of filtering ambient light to reduce the background noise seen by the system.

2.3.2.1 Laser Diodes, LEDs, and Photodiodes and Considerations for Maximum Range

One of the most fundamental questions when designing a LIDAR system is to estimate the amount of energy that the sensing element will receive as a function of the transmitted power.

Similarly to the radar equation, 式 1 is a LIDAR equation:

$$Pr = \frac{Gt \times Gr \times Pt \times \pi \times r^2}{2 \times \pi \times d^2}$$

(1)

Where:

- Gt is the efficiency of the transmitting element
- Gr is the efficiency of the receiving element
- R is the half-diameter of the optical receiving element (and $\pi \times r^2$, the surface)
- $2 \times \pi$ is the solid angle at which light is diffracted by the target
- D is the distance between the target and the sensing element

For 式 1 to hold true, assume that the transmitted light hits entirely the target. This is the role of the lenses, which are fitted in front of the laser diode or the LED.

However, keep in mind that in most industrial (and automotive) designs, the laser diode is a semiconductor diode because of their mechanical structure force the light to diffract as it leaves the semiconductor substrate (see 図 5).
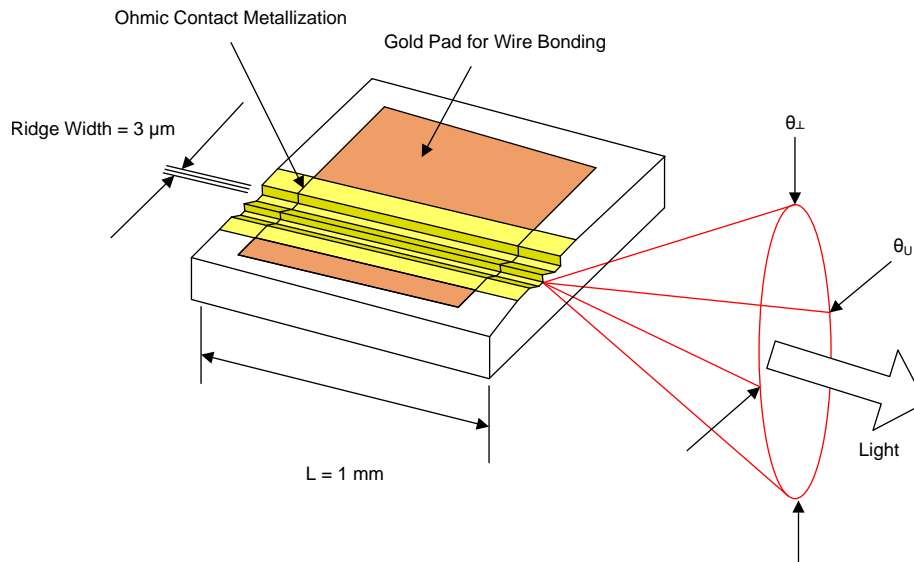

図 5. Diffraction Angles of Semiconductor Laser Diode

Most diodes being vertically stacked, the horizontal slit creates a diffracting beam that has a wider vertical angle than the horizontal angle.

As a first approximation, consider 30 to 40 degrees on the perpendicular axis and 10 degrees for the parallel axis can be considered. The lens has to be designed to fix this astigmatism; otherwise, the focal point of the perpendicular axis will not be on the same point as the focal point of the parallel axis (see 図 6).

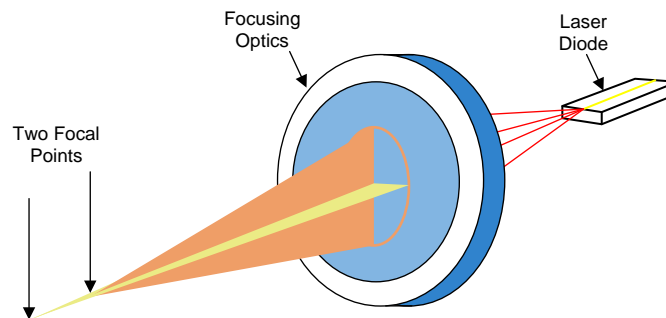**図 6. Possible Astigmatism Problem With Standard Lense in Front of Semiconductor Laser Diode**

For systems using LEDs instead of a laser diode, 式 1 needs to be corrected to factor the broad diffusion of the light. The received power is then a function of $1/d^4$ instead of $1/d^2$ for lasers.

2.3.2.2   Background Light, Wavelength, and Maximum Sensing Range

The ability to detect the echo is determined by the ability to illuminate the target and by the ability to see the illumination against background light. Background light can be inside factories, the light emitted, and diffracted by other sensors, but it could also be the light emitted by the factory lights. In outdoor environments, the background light is dominated by sunlight, whose energy density profile is given by the ASTMG173 whose profile is shown in 図 7:
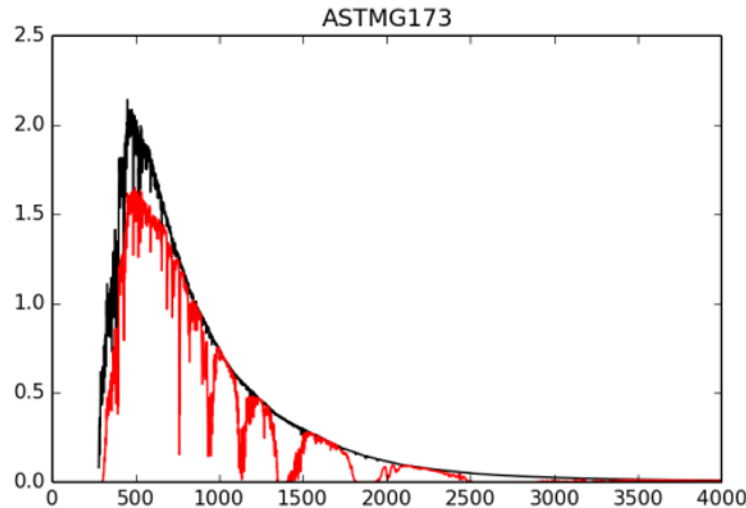

図 7. Sunlight Energy Density Profile

For indoor lighting infrared being low in LED lighting and also relatively lower than visible light, infrared is often selected as the wavelength for distance measurement.

For the outdoors, frequencies are selected as a mix between frequencies where sunlight is relatively low and availability of cost effective emitters. At the time of writing this design guide, 905 nm is the best compromise between low background light and broad availability of mass manufactured diodes and photodiodes.

When looking in the tables given by the ASTMG173, the power density at 905 nm is 0.76337 W/m ^{2}. Assuming a lense of 1.5 cm in diameter, the sensing element receives 134 µW when facing the sunlight directly.

This value though unrealistic (the uses cases for pointing a laser towards the sun are pretty thin) gives a good boundary condition for other considerations in the design.
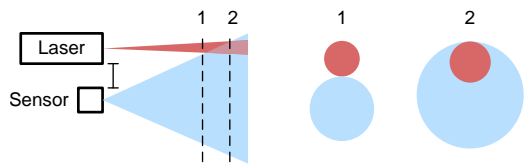
### 2.3.2.3   Attenuation Through the Air

While 905 nm is absorbed by water vapor, the contribution of attenuation through the air due to water vapor compared to the diffraction on the target is neglectable and thus is not mentioned further in this design guide.

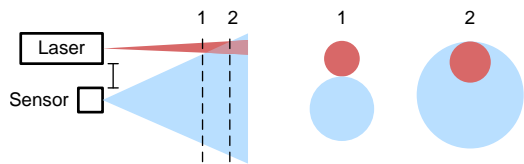### 2.3.2.4 *Reflection and Diffraction Considerations*

Many different studies focus on researching reflection and diffraction values, being dependent on the target, for different material relevant to different industries. Amongst all possible sources, this reference design cites the ISO16331, which gives boundaries for reflection to be between 20% and 80%. Riegl study gives at 905 nm, asphalt as the material with lowest relative reflectance (10%), and snow as the material with the highest relative reflectance (90%)[5].

2.3.2.5 *Field of View Considerations for Minimum Sensing Distance*

At short distances, the optics may play a strong role in defining the minimum distance that can be sensed. To ensure that the optics are designed according to the system level requirements, see 図 8.
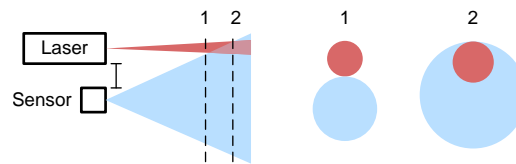
図 8. Minimum Sensing Distance

On the left of 図 8 is the laser diode, which emits a red beam. The field of view of the sensor is drawn in blue.

On the middle diagram, it is clear that the red and blue disc do not overlap. This is because the field of view of the sensor is not the same as the one of the laser emitter. As a result, no ToF computation can take place as the echo is not received by the sensor.

On the right diagram, as the field of view of both transmit and receive overlap, the sensor receives the echo and a ToF computation may be possible (assuming all other constraints are respected).

2.3.2.6 *Sensing Element*

Sensing elements are elements that convert optical power into electrical power. For a LIDAR design, the key parameters of relevance are:

- Sensing wavelength (nm): Needs to be matched to the transmit wavelength
- Responsivity (A/W): The amount of electrical current generated as a function of the optical power received. Typical values can be considered of 0.5 A/W (though varies from 0.4 to 0.7[6])
- Dark current: Because photo sensors generate current as a function of the power of light received, dark current is the current that will be generated even in absence of light.
- Rise time: The speed at which a photo sensor reacts to the optical light being received

2.3.2.7 *Eye Safety*

IEC 60825 is a key consideration for eye safety when designing with laser. Do not start a design without familiarizing with this standard.

2.3.3 Electronics for Pulse ToF

To estimate the electronics using 式 1, assume that:

- Light is perfectly collimated and 100% reaches target

- Light is perfectly diffused and 2π solid angle from the target back to the RX lense (energy density constant over $2 \times \pi \times d^2$ with d distance from target)

- RX lense r diameter (lense surface: $\pi \times r^2$)

- RX lense then capture 式 2:

$$Prx = \frac{Ptx \times \pi \times r^2}{2 \times \pi \times d^2}$$

(2)

- Ptx = 70 W

- Photo-element sensitivity of 0.5 A/W

One can compute 表 2:

表 2. Comparison of Received Power by Photo Sensor for Different Distances to Target and Associated Current Generated

d	P_RX	I_{IN}
10	80 µW	40 µA
30	9 µW	4.5 µA
100	0.8 µW	0.4 µA

From 表 2, if the assumptions listed are verified, a sensing distance of 100 m is considered achievable.

Beyond the optics, at a high-level the electronics need to fulfill the following requirements:

- Send a pulse of optical energy of the maximum amount of energy over the smallest amount of time.

- Discriminate the smallest possible amount of energy from the echo from the background noise.

- Be the most accurate possible on the time measure between the moment the light pulse is transmitted and the moment it is received.

2.3.3.1 Maximum Sensing Distance as a Function of TDC

TDCs by construct are less limited in terms of range than ADCs, which are limited to a maximum voltage and is often the supplied one. Nonetheless, TDCs have a maximum measuring range, which is their registered width. In the case of the TDC7200, its datasheet gives that the maximum range is a function of the clock fed to it.

Computing this for a few values gives:

- F = 1.0 MHz ↔ Tmax = 65.5 ms

- F = 2.0 MHz ↔ Tmax = 32.8 ms

- F = 5.0 MHz ↔ Tmax = 13.1 ms

- F = 10.0 MHz ↔ Tmax = 6.6 ms

- F = 16.0 MHz ↔ Tmax = 4.1 ms

With 4.6 ms being equivalent to 1379 km, the range of the LIDAR design is not impacted by the measurement range of the TDC.

2.3.3.2 *Resolution, Accuracy, and Repeatability*

As with any measurement system, its performances are characterized by its resolution, accuracy, and repeatability.

2.3.3.2.1 *Resolution*

The resolution of the LIDAR system is the smallest difference between two reported distances. For a TDC-based system, the resolution is determined by the LSB of the TDC.
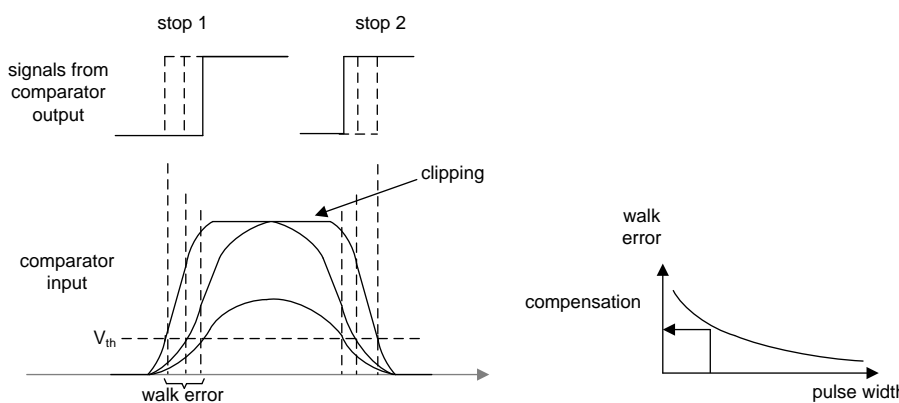
2.3.3.2.2 *Accuracy*

Accuracy is impacted by timing delays introduced over the signal chain. Those timing errors are predominantly driven by the propagation delays of the different devices. Those propagation delays vary with the following parameters: from device to device, over temperature, over supply voltage, and over input drive.

2.3.3.2.2.1 *Walk Error*

A specific accuracy error for the pulse ToF measurement is called in the literature as the "walk error." A walk error is an intrinsic source of inaccuracies resulting from combining the following factors:

- The pulse of light has a limited slope from its start until it reaches its peak of energy.
- Materials will reflect light with ratios varying between 0% and 100%.
- Pulse ToF measurement uses a threshold to detect arrival of a signal.

Given the variation of energy received, which varies with the target object and independent of the distance, the threshold will be crossed at varying times which can cause error in the estimated ToF.

This is illustrated in 図 9. The comparator input is set to the threshold voltage, V_{TH}. The bigger signal, which clips very fast, passes the threshold at t1; another signal, which barely reaches the clipping signal, will pass the threshold at time t2 (with t2 > t1); and a very attenuated signal will pass the threshold at time t3 with t3 > t2 > t1.

Those echoes are from target situated at the same distance because they peak at the same time, so the light has traveled the same distance, hence the walk error being a systematic error.
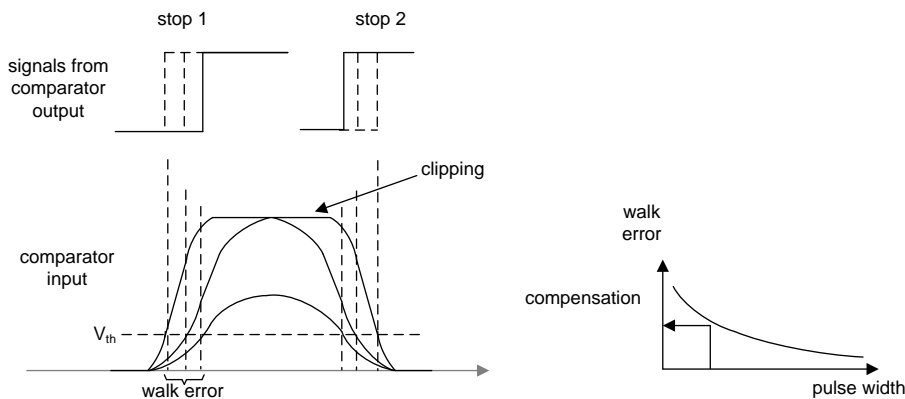

図 9. Impact of Received Amplitude on Estimated ToF and Associated Denomination of "Walk Error"

2.3.3.2.3   *Repeatability*

Repeatability is the ability of the system to provide the same result when measuring the same quantity (in other words, the relative weight of noise in the reported final value). The sources of noise in a pulse ToF system are:

- Cycle-to-cycle period jitter
- Long-term jitter
- Phase jitter
- Time interval error and maximum time interval error

It is often considered that the noise is determined by the first stage of the amplification. As most TDC architecture relies on an external clock for the "slow" counting, the external clock will contribute.

Clock noise as defined per JEDEC standard 65B JESD65V and industry best practices can be listed as:

- The background noise of the TDC component itself
- The jitter at the output of the comparator, which itself is a function of the noise at the input signal divided by the slope of the input signal

To identify the most relevant noise definition, keep in mind that the design goal for this LIDAR system is for ranges up to 100 m, which is a total ToF of 333 ns. Clocks frequencies are between 1 and 10 MHz, which means periods between 1 µs and 100 ns.

Therefore the noise contribution from the clock is the noise over one to three periods.

2.3.3.2.4   *Cycle-to-Cycle Period Jitter*

Cycle-to-cycle period jitter is defined in JEDEC Standard JESD65B as the variation in period between adjacent period, over a random sample of adjacent period pairs. While cycle to cycle is used for spread spectrum clocks rather than period jitter, it is relevant to measure the contribution of the clock to the system accuracy.

2.3.3.2.5   *Long-Term Jitter*

Long-term jitter though is not defined in JESD65B; however, it is often mentioned in literature for distance and ranging applications (sonar, LIDAR, and so on). Long-term jitter is important if the total measurement time is significantly longer than the clock period.

Given the system level requirement for this TI Design, long-term jitter is not relevant.

2.3.3.2.6   *Phase Jitter, Time Interval Error, and Maximum Time Interval Error*

Phase noise is usually specified in clocking systems, and this information is often used to derive the phase jitter or time interval error.

Phase noise is specified in dBc/Hz (where dBc is the dB relative to the carrier) and once integrated over a range of frequencies will give the noise power.

$$N = NoisePower = \int_{12\,kHz}^{20\,MHz} \pounds(f)df \tag{3}$$

From the noise power, the RMS jitter can be calculated:

$$RMSPhaseJitter(radians) = \sqrt{10^{\frac{N}{10}} \times 2} \tag{4}$$

From which the jitter in seconds can be calculated as:

$$RMSJitter(seconds) = \frac{Jitter(radians)}{2 \times \pi \times fosc}$$

(5)

2.3.3.2.7 *Allan Variance*

The generic problem of clock stability and impact on measurement has been a theoretical problem for a long time, which was eventually solved by D.W. Allan. While the considerations of the definition and applicability is beyond the scope of this reference design, find more information in the original publication[7].

2.3.4   Signal Processing for TDC

At a high level given the relative lack of publication on signal processing for TDC, this section elaborates on a few basic concepts. Some of these concepts are leveraged for this reference design, others are considered for future versions but could be used by engineers willing to start with this first reference design for LIDAR.

2.3.4.1   Review of State of the Art

Several publications[1][2][3] are using the same scheme: The received signal from the photo-detector is amplified and compared to a validating threshold of a comparator whose output triggers the STOP input of the TDC.

More advanced schemes recommend measuring the falling edge[1] to provide a compensation scheme for the walk error.

Other documents show how to make multiple ToF measurements to reduce the uncertainty of the measure (similar to oversampling and dithering techniques with ADCs).

2.3.4.2   Proposed Signal Chain for TDC-Based Setup

ADC signal processing is taught in all electronic classes and is based on the sampling theory of Harry Nyquist and the later work of Claude Shannon, published in 1948 in the paper "A Mathematical Theory of Communication," resulting in the Nyquist-Shannon sampling theorem.

To work with the digital samples coming from the TDC, one has to look at the problem from another angle. 表 3 gives an overview of the differences and similarities.

表 3. Comparing ADC-Based Sampling and TDC-Based Sampling

PARAMETER	ADC-BASED SAMPLING	TDC-BASED SAMPLING
Conversion trigger	Clock input (either internal or external) or trigger	Level crossing
Analog signal amplitude information	Exact to the quantization error	Exact but lower number of steps
Digital output	Digital image of the input voltage	Digital image of the time at the instant of crossing the threshold
Main noise characteristics	Voltage noise	Jitter

Before looking into the signal processing specifics of the TDC generated samples, another important consideration is to get familiar with a lesser known publication from the Bell Labs. In 1976, B.F. Logan published the article "Information in the Zero Crossings of Bandpass Signals" in which he demonstrated that at the zero crossings of h determine h within a multiplicative constant.

In other words, if one has a bandpass signal and captures the instant at which the signal crosses zero, one has all the required information to reconstruct the signal except for the amplitude.

Based on this, one can reasonably start building a TDC based system that captures rising edges and falling edges when crossing the zero and, knowing that all the information is given, process it to extract the desired ToF.

2.3.4.3   *Time Domain Correlation*

not having found an existing name for the described method, the author offers that the following be called "time domain correlation." Time domain correlation takes the samples from the TDC (having sampled rising and falling edges at the zero cross) for both the transmit and for the receive signal.

Time domain correlation has the following benefits:

* Optical multi-path detection
* Increased SNR

To reject optical multi-path (or to detect them), the transmit pattern must be a form of orthogonal codes and the receiver only needs to correlate with the last transmitted pattern.

To detect optical multi-path, the receiver needs to store in a buffer the patterns and try the patterns that are stored in the buffer.

This concept is illustrated in the following diagrams.
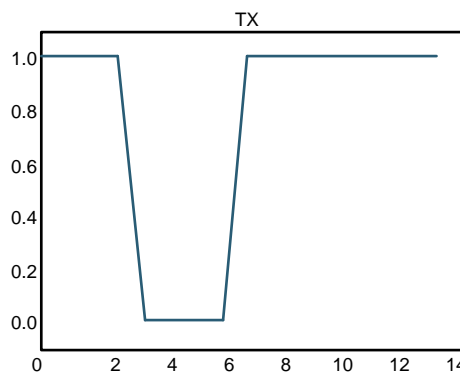
図 10. Transmit Pattern (Time Unit is Arbitrary): 1-1-0-0-1-1-1-1

In absence of any noise, the output of the comparator would be the one shown in 図 11.
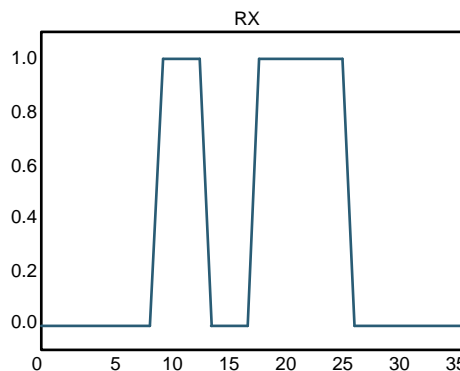
図 11. Output of the Comparator in Absence of Noise

Once the MCU reads the TDC values, the memory will hold [10,+],[14,–],[17,+]… where the number is the time stamp and the symbol is the rising or falling edge. A very simple subroutine could expend this into an array, which would resemble 図 11.

Assuming now that the signal chain is noisy, look at a possible output of the comparator as shown in 図 12.
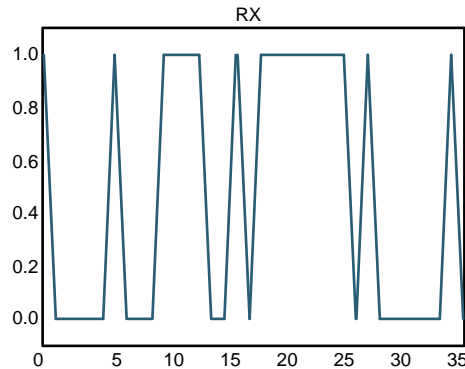
図 12. Output of the Comparator Feeding the TDC in Presence of Noise

Typically, the threshold of the comparator is selected three times above the RMS noise floor (or six times depending on the compromise between false positive and false negatives). With the proposed approach, the threshold can be lowered significantly, thus reducing the amount of false negatives. With a classical approach, however, the MCU subroutine may consider a ToF of 5 of the arbitrary time unit.

However, after computing a simple cross correlation between both the noise free received signal and the noisy received signal (see 図 13), the correct ToF (10 arbitrary units) is correctly computed in both cases.
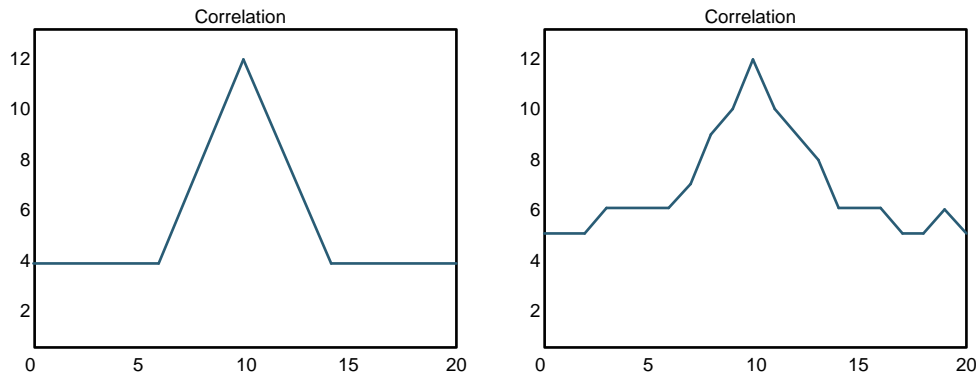
図 13. Correlation Between Received Signals and Transmitted Signals (Respectively Noise Free and Noisy)

2.3.4.4   *Signal-to-Noise Ratio*

A signal-to-noise ratio is defined as the ratio of the power of the signal to the power of the background noise (or unwanted signal).

For a TDC-based signal chain, take care when selecting the detection threshold when the electrical level passes it, meaning that the signal has being detected.

When a single event is to be detected (the generating and processing of a single STOP signal), the threshold needs to be selected so that the probability of a false positive is acceptable for system performances.

As a reminder, the instant value of a white Gaussian noise is higher than its standard deviation (also called RMS value) such that a signal is 16%. Therefore, if a system can accommodate more than 16% of false ToF results (either through averaging or through robustness at other levels of the system), the threshold at the input can be set to the background noise level average plus its RMS value.

Assuming that the background noise has a mean value of zero, in the following table is summarized the system robustness.

表 4. False Trigger

V_{TH} AS A FUNCTION OF RMS	PROBABILITY OF FALSE TRIGGERING OF TDC
1	16%
2	2.3%
3	0.13%

Given the white Gaussian nature of the considered noise, the time of triggering will be equally distributed between 0 and the theoretical ToF arrival.

Being able to measure multiple STOP pulses can help to increase robustness because sets of pulses that are not spaced by the transmit pattern can be rejected.

Moving from detecting a single pulse rising edge to detecting all the zero cross can further improve the SNR. It is possible to use the theoretical framework setup by Logan by selecting an arbitrary amplitude of one for all signal. The SNR, which is beyond the ratio of power, is the ratio of the square of the amplitude. Having selected an arbitrary amplitude of '1' (one), the SNR then becomes the ratio of the square of the pulse widths:

$$\text{SNR} = \frac{\text{Psignal}}{\text{Pnoise}} = \frac{V^2\text{signal}}{V^2\text{noise}} = \frac{\sum t^2\text{signal}}{\sum t^2\text{noise}}$$

(6)

In other words, in the time domain, the SNR is the ratio of the square of the pulse width time of signals to the square of the pulse width of the noise.

2.3.4.5   *Additional Benefit of Time Domain Correlation*

An additional benefit of the proposed scheme is that it also allows to compute a compensation scheme for the walk error[1].

3 Testing Requirements and Test Results

3.1 Test Setup

This reference design is in a BoosterPack™ form factor. This allows the design to connect to a TI LaunchPad™ to use and evaluate easily. The chosen LaunchPad is the one that contains the MSP430FR5969, which is a 16-MHz ultra-low-power microcontroller featuring a 60KB FRAM, a 2KB SRAM, and 40IO. The microcontroller initiates the sequence that triggers the two TDC7200 devices, which measure the time taken by the light to fly back and forth to an object, and the UCC27321, which drives the laser.

In this reference design, the main focus has been to characterize the differential ToF measurements approach using two TDC7200 devices. To do that, the error of the differential measurement of the two TDC7200 devices has to be calculated. The error is nothing else than the difference of the ToF, which is the time passed between the START and the STOP pulses, of the two TDC7200 devices once they receive exactly the same START and STOP pulse.

The TDC7200 has a blanking time of 12 ns. This blanking time is too big for small distance sensing. This reference design allows virtually no blanking time for TDC measurement.

図 14 shows the test setup. A pulse trigger is generated by a GPIO pin of the LaunchPad. This pin is connected to the START pin of the two TDC7200 devices and to the TRIG input of a waveform generator, HP33250A.

After receiving a START pulse, the clock counter of the TDC7200 starts after the next rising edge of the external clock signal that comes from the MSP430FR5969. This can be set to 1 MHz, 4 MHz, and 16 MHz.

At the same time, the waveform generator, after receiving the START pulse, generates a delay set by the user and outputs a STOP trigger, which is sent back to the STOP pin of the two TDC7200 devices through SMA cables of the same length.

After the STOP trigger has been received, the TDC signals to the MCU through interrupt (INTB pin) that there are new measurement results waiting in the registers. If no STOP signal is received, either the Clock Counter or Coarse Counter overflow and generate an interrupt.

Depending on the expected ToF, the TDC7200 can be configured in two different modes. Measurement mode 1 is for an expected ToF that is smaller than 500 ns while measurement mode 2 is for an expected ToF that is bigger than 500 ns. Depending on the chosen measurement mode, there are two different way to calculate the ToF:

$$TOF_n = (TIME_n)(normLSB) \tag{7}$$

$$TOF1 = (TIME1)(normLSB) + (CLOCK\_COUNT1)(CLOCKperiod) - (TIME2)(normLSB) \tag{8}$$

For more information about these measurement modes, see *TDC7200 Time-to-Digital Converter for Time-of-Flight Applications in LIDAR, Magnetostrictive and Flow Meters*.

To measure the differential measurements of the two TDC7200 devices for this reference design, use measurement mode 2 even for a ToF below 500 ns.

Calibrate to know the actual value of the LSB, normLSB. Keep in mind that the actual value of the LSB can vary depending on environmental variables (temperature, systematic noise, and so on). This variation can introduce significant errors into the measurement result. There is also an offset error in the measurement due to certain internal delays in the device.
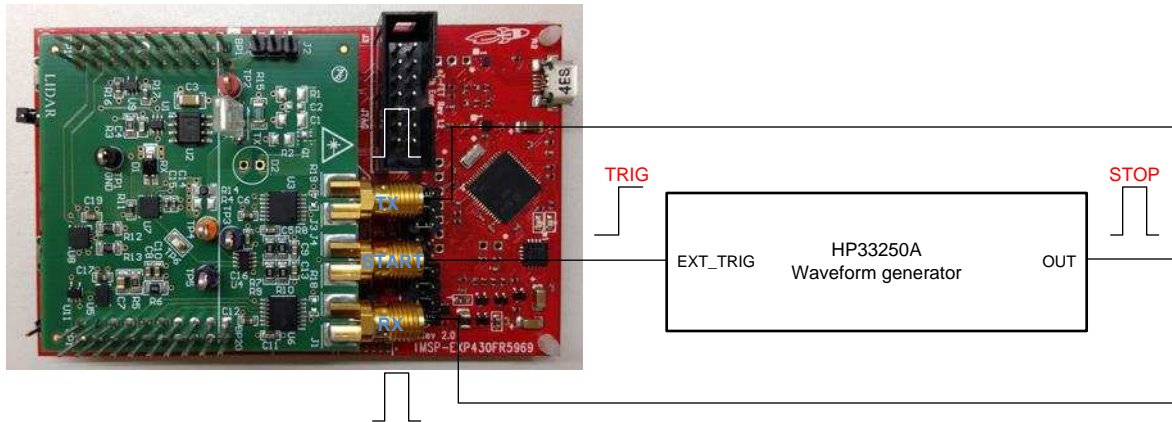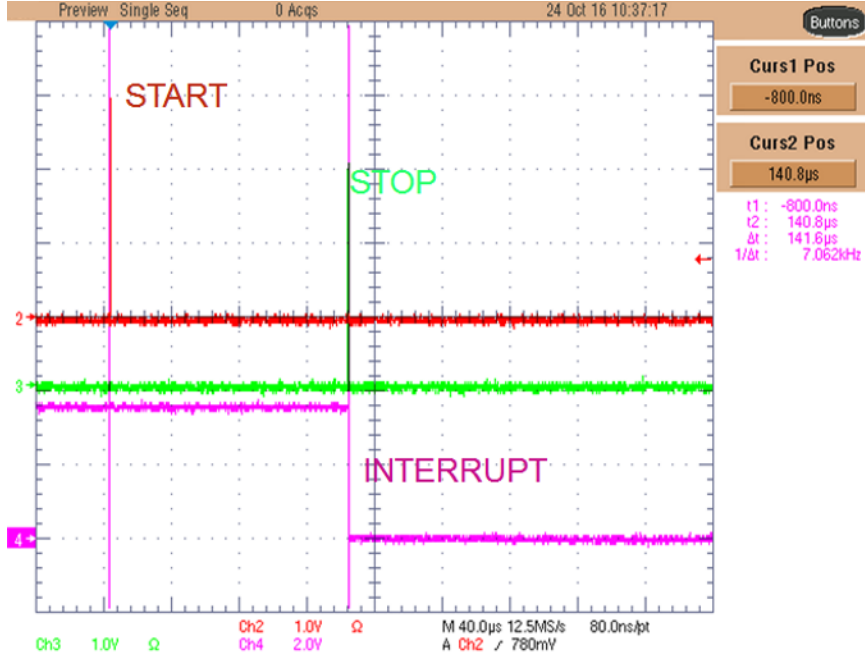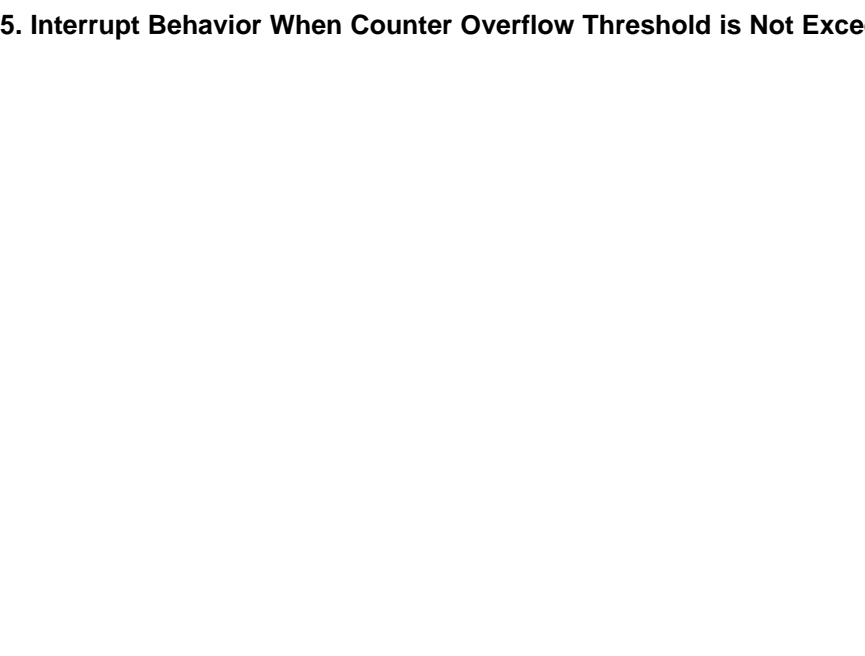
図 14. Test Setup

3.2 Test Results

The interrupt status of the two TDCs has been monitored through an oscilloscope to check that the TDC signals the MCU correctly MCU once the STOP trigger has been received.

The counter overflow threshold have been set to 250 μs. In 図 15, the threshold is not exceeded, meaning that the interrupt (green line) is generated once the TDCs receive the STOP trigger. In 図 16, the threshold is exceeded, meaning the interrupt is generated once the clock reaches 250 μs and no STOP (red line) trigger is received yet.
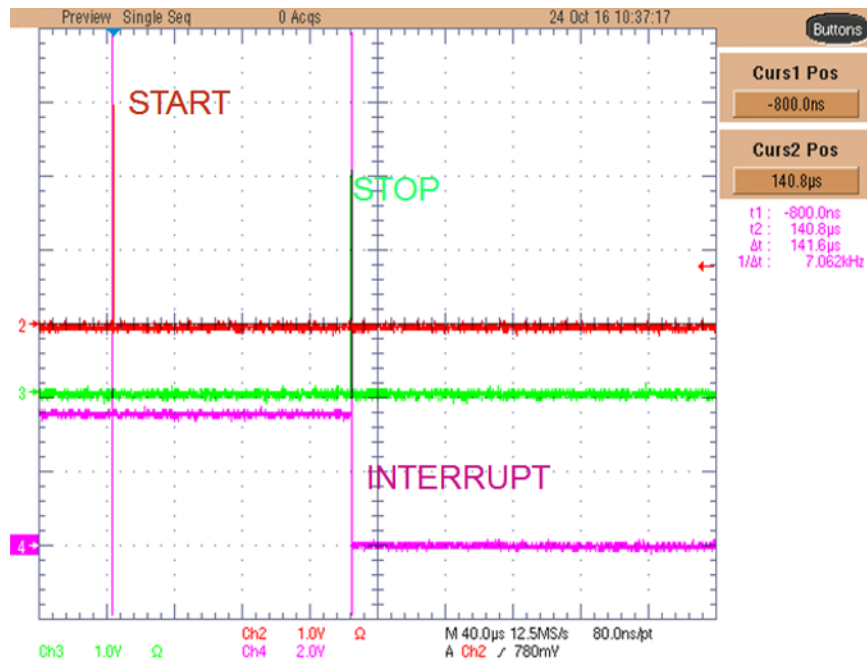
図 15. Interrupt Behavior When Counter Overflow Threshold is Not Exceeded
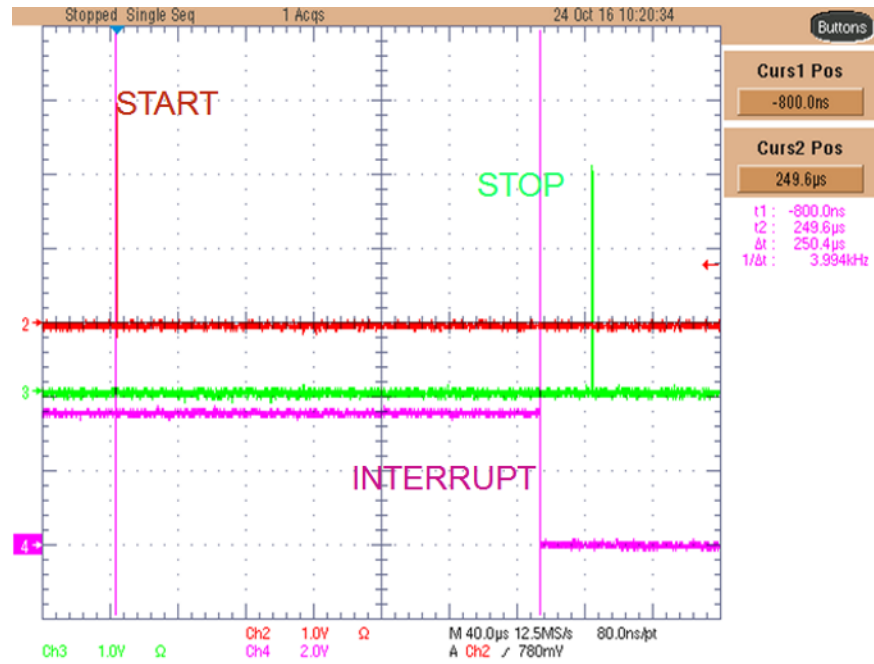
図 16. Interrupt Behavior When Counter Overflow Threshold is Exceeded

The delay between the START and STOP trigger varies from 20 up to 140 µs with steps of 20 µs with the waveform generator, and for each step, the error as a difference between the measured ToF of the two TDCs is calculated.

This calculation has been done feeding to the TDC three different clock frequency coming from the MSP430FR5969 (1 MHz, 4 MHz, and 16 MHz). The results are shown in 図 17, 図 18, and 図 19, where on the y axis is represented the error and on the x axis is represented the delay generated by the waveform generator.
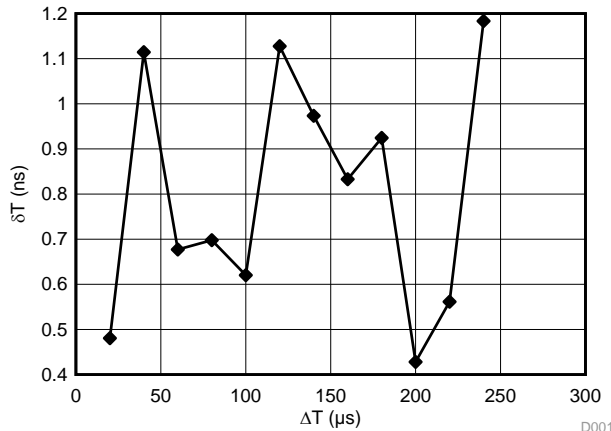
図 **17. Differential Error With 1-MHz Clock**
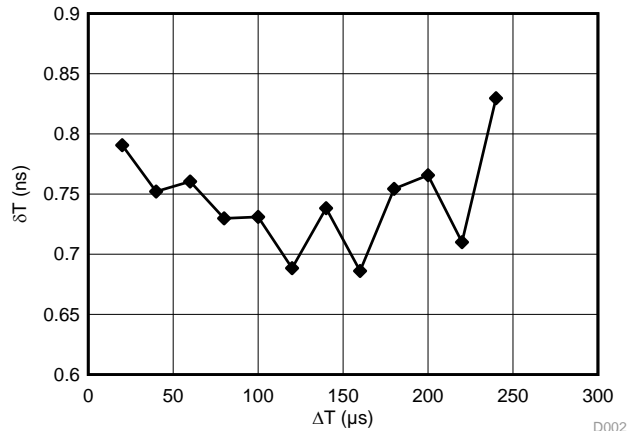
図 **18. Differential Error With 4-MHz Clock**
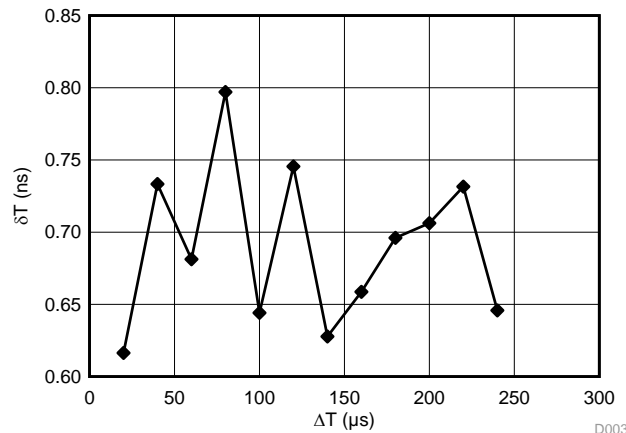
図 **19. Differential Error With 16-MHz Clock**

As shown in these graphs, the error decreases as the clock frequency increases. This is true because the standard deviation of the TDC decreases as the clock frequency increases. At 16 MHz, the system differential error related to the hardware itself is 800 ps peak to peak. It is important to notice that the following contributed to this error: the HP33250A, which has a trigger input burst jitter (RMS) of 1 ns, the accuracy of the internal clock of the MSP430FR5969, and some cabling mismatch.

The jitter accumulates on each clock cycle, so the uncertainty associated to a time measurement is a function of the clock jitter and the number of clock cycles measured. Averaging can be improved by reaching an error below 30 ps, which corresponds to less than 1 cm.

4 Design Files

4.1 Schematics

To download the schematics, see the design files at TIDA-00663.

4.2 Bill of Materials

To download the bill of materials (BOM), see the design files at TIDA-00663.

4.3 PCB Layout Recommendations

4.3.1 Layout Prints

To download the layer plots, see the design files at TIDA-00663.

4.4 Altium Project

To download the Altium project files, see the design files at TIDA-00663.

4.5 Gerber Files

To download the Gerber files, see the design files at TIDA-00663.

4.6 Assembly Drawings

To download the assembly drawings, see the design files at TIDA-00663.

5 Software Files

To download the software files, see the design files at TIDA-00663.

6 Related Documentation

1. Optical Engineering, *Laser ranging: a critical review of usual techniques for distance measurement* , 40:10-19
2. University of Oulu, *Integrated Receiver Channel and Timing Discrimination Circuits for a Pulsed Time-of-flight Laser Rangefinder*
3. IEEE, *A 9-channel Time-to-Digital Converter for an Imaging Lidar Application*
4. Chalmers University of Technology, *Development of a low-cost laser range-finder (LIDAR): Master's Thesis in Systems, Control and Mechatronics*
5. RIEGL, *Multi-Wavelength Airborne Laser Scanning*
6. University of Washington, *Optical Detectors*
7. Allan, D. W., *Conversion of Frequency Stability Measures from the Time-domain to the Frequency-domain, vice-versa and Power-law Spectral Densities*

6.1 商標

E2E, MSP430, BoosterPack, LaunchPad are trademarks of Texas Instruments.
すべての商標および登録商標はそれぞれの所有者に帰属します。

7   Terminology

TDC—   Time-to-digital convertor

> To better understand the TDC name, consider an ADC as being a "voltage-to-digital converter." ADCs are used to convert the physical unit "volts" into a digital image, which is usually proportional to an absolute reference. Similarly, TDCs are a sub-branch of the ADC realm that focus on converting the physical unit "time" into a digital value.

8   About the Authors

MATTHIEW CHEVRIER is a systems architect at Texas Instruments, where he is responsible for defining and developing reference design solutions for the industrial segment. Matthieu brings to this role his extensive experience in embedded system designs in both hardware (power management, mixed signal, and so on) and software (such as low level drivers, RTOS, and compilers). Matthieu earned his master of science in electrical engineering (MSEE) from Supélec, an Ivy League university in France. Matthieu holds patents from IPO, EPO, and USPTO.

GIOVANNI CAMPANELLA is a systems engineer at Texas Instruments, where he is responsible for defining and developing reference design solutions for the industrial segment. He earned his bachelor's degree in electronic and telecommunication engineering at the University of Bologna and his master's degree in electronic engineering at the Polytechnic of Turin in Italy. He is an expert in sensors and analog signal chain, with a focus on magnetic and analytics sensing technologies and mixed-signal control of DC brushed servo drives.

8.1   *Acknowledgments*

The authors wish to thank **SAMIR CHERIAN** for his help all through this project on all key aspects of the OPA857. Without Samir, this project would not have been possible in the given timeline.

改訂履歴

資料番号末尾の英字は改訂を表しています。その改訂履歴は英語版に準じています。